Sensors and Materials, Vol. 37, No. 5 (2025) 2081–2090
MYU Tokyo

S & M 4043

Using Simulation Method to Analyze Intraocular Pressure at Different Postures and Eye Movement Angles

Jiehui Zheng,[1] Chih-Chung Cheng,[2] Chao-Ming Hsu,[2] Chia-Wen Lee,[1] Pei-Chang Wu,[3,4] Linda Yi-Chieh Poon,[3,4*] and Cheng-Fu Yang[5,6**]

[1]School of Information Engineering, Xiamen Ocean Vocational College, Xiamen 361102, China
[2]Department of Mechanical Engineering, National Kaohsiung University of Science and Technology, Kaohsiung 807, Taiwan
[3]Department of Ophthalmology, Kaohsiung Chang Gung Memorial Hospital, Kaohsiung 833, Taiwan
[4]School of Medicine, Chang Gung University, Taoyuan 333, Taiwan
[5]Department of Chemical and Materials Engineering, National University of Kaohsiung, Kaohsiung 811, Taiwan
[6]Department of Aeronautical Engineering, Chaoyang University of Technology, Taichung 413, Taiwan

(Received January 27, 2025; accepted April 17, 2025)

Keywords: intraocular pressure (IOP), Ansys, SolidWorks, stress and strain, Mooney–Rivlin hyperelastic material, standing, side-lying, supine

In this project, we analyzed the stress and strain distributions in the eye under pressure using Ansys finite element simulation software, with the eye model created in SolidWorks. We simulated contact tonometry by applying various probe forces to measure intraocular pressure (IOP) changes. Five different eye models with axial lengths ranging from 22 to 30 mm were investigated. The process began with creating detailed eye components in SolidWorks, including the aqueous humor, zonular fibers, ciliary body, sclera, cornea, and vitreous body. These components were then imported into Ansys for mesh generation, boundary condition definition, and simulation calculations. Results were analyzed using the Ansys postprocessor and validated against experimental measurements to ensure accuracy. For material properties, all eye tissues were modeled as Mooney–Rivlin hyperelastic materials. During compression, the cornea and sclera were found to be the primary structures absorbing the concentrated loads. The simulation examined three patient positions, namely, standing, side-lying, and supine, combined with eyeball rotations of 15, 30, and 45°. This comprehensive approach allowed for the observation of stress-strain relationships and IOP variations under different probe forces and eye orientations.

1. Introduction

The World Health Organization has designated glaucoma as one of the primary targets in its 2020 global blindness prevention initiative, recognizing it as a leading cause of vision loss worldwide.(1) Individuals with elevated intraocular pressure (IOP) face a higher risk of optic nerve damage that can progress to glaucoma than those with normal pressure. Glaucoma develops when IOP exceeds the tolerance threshold of the optic nerve. These pressure fluctuations are primarily affected by the balance between aqueous humor production and

*Corresponding author: e-mail: lindap@cgmh.org.tw
**Corresponding author: e-mail: cfyang@nuk.edu.tw
https://doi.org/10.18494/SAM5566

ISSN 0914-4935 © MYU K.K.
https://myukk.org/

drainage rates. While the normal IOP typically ranges from 10 to 20 mmHg,[2] it is important to note that most cases of glaucoma progress without clear symptoms, leading to low public awareness. Unfortunately, by the time damage is detected, optic nerve atrophy has often already occurred. Regarding IOP, there is no absolute safe threshold. Some individuals maintain pressure readings within the normal range yet experience progressive optic nerve changes, while others with elevated pressure show no signs of optic nerve damage. This variability demonstrates that elevated IOP, while being the only measurable and controllable factor, is just one of several elements contributing to glaucoma development.

The measurement and detection of IOP is a complex science that has evolved significantly from early contact-based methods to modern noncontact tonometers. While these newer methods offer greater convenience and reduce infection risks through contact, measurement accuracy can still vary owing to differences in underlying principles and equipment specifications. Previous intraocular surgeries, residual fluids or gases in the eye, and laser vision correction procedures can all affect measurement accuracy, leading to either the overestimation or underestimation of pressure readings. Whether by contact or noncontact methods, these techniques typically involve applying a fixed force to the cornea and calculating the degree of indentation or deformation. Such measurements are affected by several factors, including central corneal thickness (CCT), corneal curvature (K), and corneal biomechanical properties. Among these factors, corneal thickness has the most significant impact on pressure readings. Patients with thicker corneas may show falsely elevated readings, potentially leading to incorrect glaucoma diagnoses. Conversely, those with thinner corneas might have their pressure underestimated, resulting in glaucoma being misdiagnosed as normal-tension cases. While noncontact tonometry avoids corneal deformation and reduces corneal influence, it paradoxically shows greater measurement variability than contact methods.

Related congenital syndromes may also be associated with abnormalities in CCT, which can affect the accuracy of IOP measurements. IOP is higher in the supine position than in the upright position, with differences ranging from 0.3 to 6 mmHg. These pressure variations are more pronounced in glaucoma patients than in normal individuals. After lying down, pressure can increase for 30 to 60 min, but it returns to baseline once the person sits up again.[3,4] The mechanism behind the elevated IOP in the supine position may involve two factors: increased scleral venous pressure and the congestion of the uveal blood vessels. Changing the scleral volume modulus from 0.1 to 1 GPa has minimal impact on all model parameters. When IOP increases from 30 to 45 mmHg, displacement across all directions is minimal. This suggests that the sclera is relatively compliant at IOPs between 5 and 10 mmHg, but becomes significantly stiffer as the pressure rises above 30 mmHg. For a 50° horizontal rotation of the eye, the maximum forces generated by the lateral and medial muscles are, on average, 580 and 730 mN, respectively.

There is a nonlinear relationship between the range of eye rotation and the level of muscle activity, meaning that when the eye rotates 13°, the corresponding muscle forces will be less than 151 and 190 mN.[5,6] During horizontal eye movement, the force generated by the medial muscle is generally greater than that produced by the lateral muscle. Assuming a corneal strain of 18%, a scleral strain of 6.8%, and a stress of 9.4 MPa when rupture occurs, with the vitreous body having a hydrostatic pressure of 20 mmHg (2.7 kPa), the Poisson's ratio between the sclera and the cornea ranges from 0.395 to 0.48.[7] Additionally, it has been observed that the maximum horizontal rotation speed of the human eyeball is 900°/s, which occurs during a 30° saccadic eye movement.[8] However, in modern life, almost everyone checks their phones before bed, which contributes to the increasing trend of younger individuals developing glaucoma. The motivation for these simulations is to identify a posture angle that results in a relatively lower increase in IOP. In this study, we used Ansys simulations to model the deformation of the eyeball under pressure, considering different postures and positions.[9] In recent years, the incidence of glaucoma has increased by 20 to 30% among individuals aged 20 to 40. Owing to the effects of gravity, IOP is higher in the supine position than in the seated or standing position. Furthermore, with modern habits, almost everyone checks their phone before bed, which is one of the reasons why glaucoma is becoming more common among younger individuals. The motivation behind this simulation is to identify posture and eye movement angles in which IOP increases less, in comparison with other positions.

2. Methodology

In this study, the eyeball dimensions were based on typical adult measurements. First, using SolidWorks drawing software, the aqueous humor, suspensory ligament, ciliary body, cornea, sclera, and vitreous body were modeled and combined, as shown in Fig. 1(a). The model was then imported into Ansys for finite element preprocessing. The mesh generation was performed using the mesh module in Ansys, as shown in Fig. 1(b). Ansys's built-in material models were used, requiring the input of elastic and physical parameters such as density, Poisson's ratio, and Young's modulus, as well as material-specific constants such as the Mooney–Rivlin 2 parameter

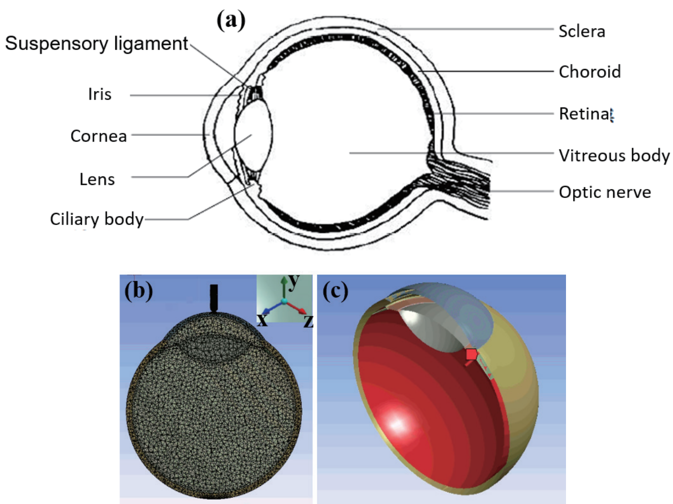

Fig. 1. (Color online) (a) Simple illustration of eyeball, (b) eyeball grid map, and (c) application of pressure to inner wall of eyeball.

and the equation of state. The eye model was created in SolidWorks with the following dimensions: the anterior lens curvature radius was 10 mm, the corneal curvature radius was 7.8 mm, the scleral radius was 11.25 mm, and the posterior lens curvature radius was 6 mm. A probe was used to apply force to the eyeball to simulate the internal pressure changes. The simulation was carried out using Ansys Workbench 19.0. Material properties necessary for the pressure analysis of the eyeball were specified, including those for the vitreous body, suspensory ligament, cornea, sclera, ciliary body, and aqueous humor. The material properties for the cornea and sclera were obtained from existing literature, while the suspensory ligament and ciliary body were modeled using Mooney–Rivlin elastomers. During compression, the cornea and sclera primarily absorbed the concentrated load applied during pressure changes.

The relationship between the cornea and the sclera is modeled as a single entity, with the contact surface between the probe and the cornea assumed to be frictionless. Because of the frictionless assumption, the probe might slide. To prevent this, the probe was fixed by setting displacements along the x- and z-axes to 0, while allowing free displacement along the y-axis, as shown in Fig. 1(b). Rotations along all three axes were also set to 0, and loads and boundary conditions were defined through the load module, which were associated with the analysis steps. In the load configuration, the probe was subjected to five different force values, namely, 9.81, 19.62, 29.43, 39.24, and 49.05 mN, corresponding to IOPs of 10, 20, 30, 40, and 50 mmHg, respectively. Since IOP is the pressure exerted on the inner surface of the eyeball, the load was applied to simulate the pressure on the sclera, as shown in Fig. 1(c). The IOP was set as 1.33, 2.66, 3.99, 5.32, and 6.65 kPa. In this study, we conducted a convergence analysis by establishing different element numbers in combination with remesh functionality. The overall model, assuming a supine position, focused on the contact point between the cornea and the probe for the convergence analysis. Since the model involved curved surfaces, and to achieve the minimum element count for solver convergence, an initial reference of 200000 elements was used, with the element count gradually increased. The simulation results showed that the stress on the cornea remained within a 1% error range when the element count was between 400000 and 500000. Therefore, an element count of 400000 was chosen for the final analysis.

3. Simulation Results and Discussion

First, practical measurements were conducted using a titanium alloy probe, and the changes in equivalent stress and strain in the cornea under pressure were analyzed. The measurement results showed that as the applied pressures were 1.33, 2.66, 3.99, 5.32, and 6.65 kPa, the strain in the cornea progressively changed as 0.091, 0.11, 0.13, 0.14, and 0.15 mm/mm, respectively, demonstrating a gradual increase. Simultaneously, the equivalent stress measured in the cornea also increased with pressure, with values of 0.087, 0.114, 0.138, 0.177, and 0.195 MPa. Additionally, when measurements were taken at the optic nerve position, the equivalent stress ranged from 1.5 to 2.8 kPa, with corresponding strain varying between 0.00054 and 0.00058 mm/mm. These results indicate that, although the changes in equivalent stress and strain at the optic nerve position were relatively small, there was still a notable shift in local force distribution as the applied pressure increased. From these results, it is evident that as the titanium alloy probe exerts pressure on the cornea, both the strain and equivalent stress in the cornea gradually increase with the applied external force. This suggests that the cornea, as part of the eye, responds predictably to external pressure, with its deformation also increasing with pressure.

This may potentially impact the structural stability and functionality of the eye. Although the strain changes at the optic nerve position were relatively small, attention must still be paid to the pressure conditions in this area. The optic nerve is a crucial structure in the eye, and an excessively high pressure in certain cases can cause damage to it. Therefore, special care should be taken in clinical procedures to monitor the pressure distribution in these regions. There is a certain correlation between the degree of myopia and axial length. Research shows that for every 300° increase in the degree of myopia, the eye's axial length extends by approximately 1 mm. The IOPs under eye axial lengths of 22, 26, and 30 mm are illustrated in Figs. 2(a)–2(c), respectively (with data for 24 and 28 mm not shown). These measurements were taken using a titanium alloy probe to simulate three different postures: supine, standing, and prone. The simulated eye types include hyperopic eye, emmetropic eye, myopic eye with −600D, myopic eye with −1200D, and myopic eye with −1800D. In these figures, the *X*-axis represents the

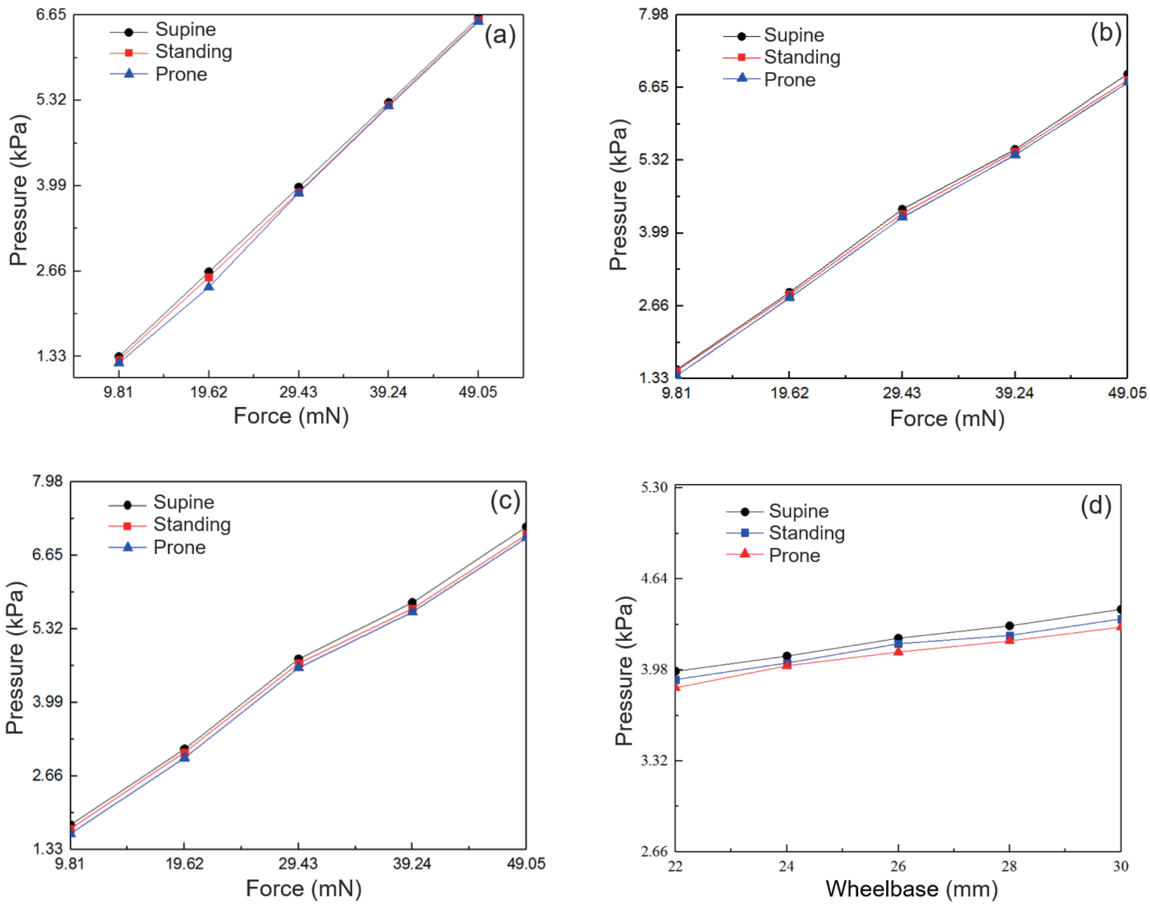

Fig. 2. (Color online) Relationships between eye axial length and IOP for different postures: (a) 22, (b) 26, and (c) 30 mm. (d) Comparison of IOP results for five different axial lengths with a force of 29.43 mN.

applied force, while the *Y*-axis represents the corresponding IOP. Figure 2(d) shows the IOP results with an applied force of 29.43 mN. From this figure, it is clear that as the axial length of the eye increases, the IOP also tends to rise. This suggests that the longer the axial length of the eye, the higher the IOP.

Furthermore, when comparing the IOP across the three postures, the supine position shows the highest IOP, followed by the standing position, and the prone position with the lowest. This reflects the effect of different postures on IOP, with the supine position possibly increasing the distribution of intraocular fluids and raising the IOP due to gravitational effects. These findings demonstrate that the axial length has a significant impact on the IOP. As the axial length increases, the IOP rises, which has important implications for the treatment and management of myopia. A chronic high IOP may adversely affect the structure of the eye and potentially lead to ocular diseases such as glaucoma. Therefore, understanding the effects of different axial lengths and postures on the IOP is crucial for clinical diagnosis and treatment. Additionally, the effect of posture, especially the higher IOP observed in the supine position, suggests that posture should be considered during clinical examinations. In future research, one can further explore the patterns of IOP changes in different postures and integrate individual ocular structural characteristics to develop more precise IOP management strategies.

In this section, we primarily examine the effect of corneal thickness on the accuracy of IOP measurements. In the study, we focused on the relationship between the force applied by the probe and the changes in IOP, based on the corneal thickness parameters set in this research. A normal, nonmyopic eyeball with an axial length of 24 mm was selected as the eye model, and a titanium alloy probe was used. By varying the corneal thickness parameters, different scenarios of IOP measurements were simulated. Figures 3(a)–3(c) illustrate the simulated IOP values in supine, standing, and prone positions, with the corneal thickness set at 0.5, 0.55, and 0.6 mm, respectively. From these figures, it is evident that as the corneal thickness increases, the simulated IOP values show a gradual decline. However, the actual measurement process contradicts this trend. In reality, as the corneal thickness increases, the measured IOP tends to be higher. This discrepancy arises because when using a tonometer for IOP measurement, the instrument flattens the cornea to a fixed area, approximately 3.06 mm^2, during the process. The increased corneal thickness affects the resistance to indentation, which results in higher IOP readings when measured. Therefore, the difference in corneal thickness must be considered when interpreting IOP measurements, especially in clinical settings, to avoid inaccurate readings that could lead to misdiagnosis or improper treatment decisions. This highlights the importance of understanding the relationship between corneal characteristics and IOP measurements for improved diagnostic accuracy.

As the cornea becomes thicker, the force required to flatten it to a fixed area increases, which results in a higher measured IOP. In contrast, the force applied during the simulation process is constant and affected by material parameters, creating a certain disparity compared with real-life conditions. Therefore, the impact of corneal thickness on IOP presents an opposite trend in the simulation compared with actual measurements. In summary, there is a significant difference in how corneal thickness affects IOP in simulations versus real-world measurements. In the simulated environment, an increase in corneal thickness leads to a decrease in IOP, while in

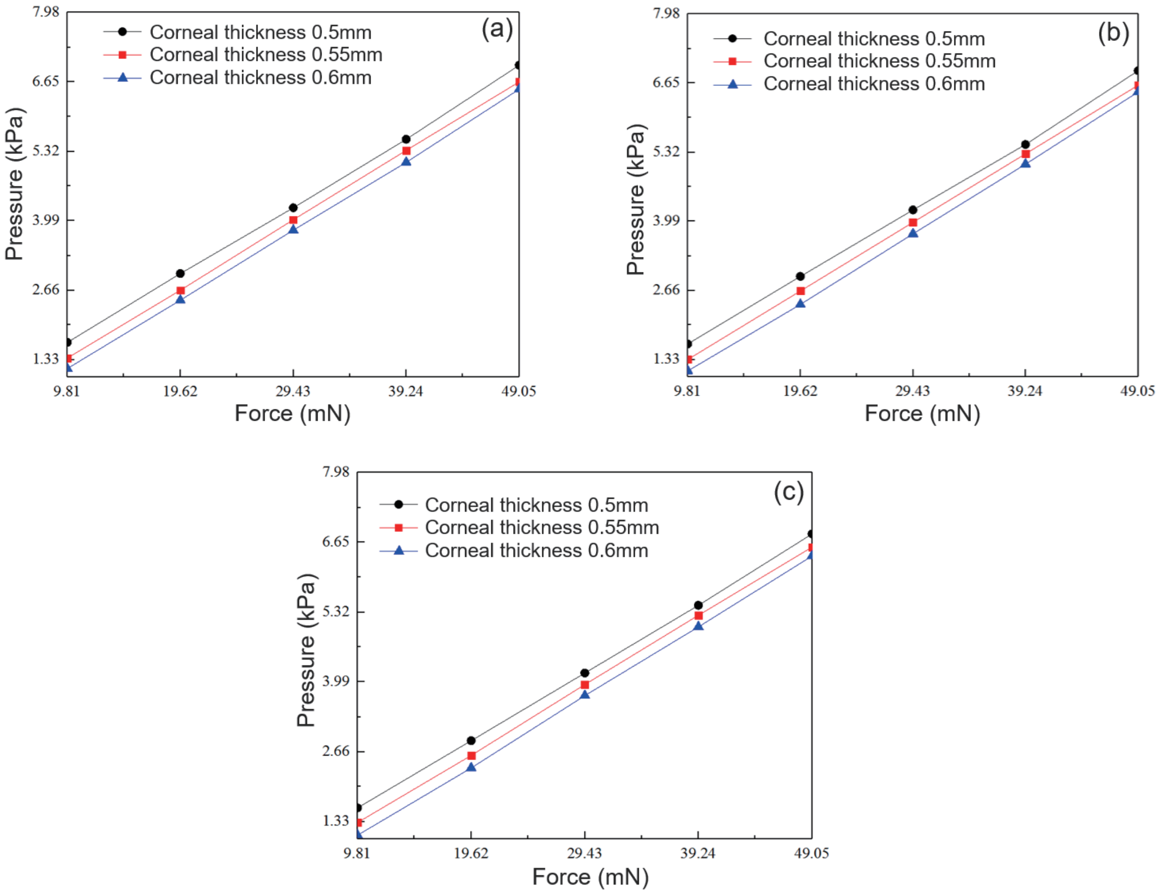

Fig. 3. (Color online) Relationships between force and IOP for different postures: (a) supine, (b) standing, and (c) prone.

reality, the tonometer applies additional pressure to flatten the thicker cornea, which results in a higher IOP reading. This phenomenon underscores the importance of considering corneal thickness as a factor that can affect the accuracy of IOP measurements in clinical practice. It may also necessitate further compensatory or corrective measures to enhance the accuracy of IOP readings. The correction formula for IOP based on corneal thickness is as follows.[10]

$$Corrected\ IOP = Measured\ IOP + (550 - CCT) \times 0.04 \quad (1)$$

This formula is used to correct the relationship between the measured and true IOPs. The formula assumes a standard corneal thickness of 550 µm. For every 50 µm increase in corneal thickness, the measured IOP is overestimated by 2 mmHg, so a correction of subtracting 2 mmHg is applied to obtain a more accurate IOP. Conversely, for every 50 µm decrease in corneal thickness, the measured IOP is underestimated by 2 mmHg, requiring an addition of 2 mmHg to restore the true IOP. This correction reveals that the relationship between the force applied and the IOP shows a linear trend, meaning that the force applied is proportional to the change in IOP. Additionally, different postures can affect IOP measurements, as posture changes affect the external pressure exerted on the eyeball and alter blood circulation, which in turn impacts the IOP. Therefore, to enhance the accuracy of IOP measurements, it is essential to not

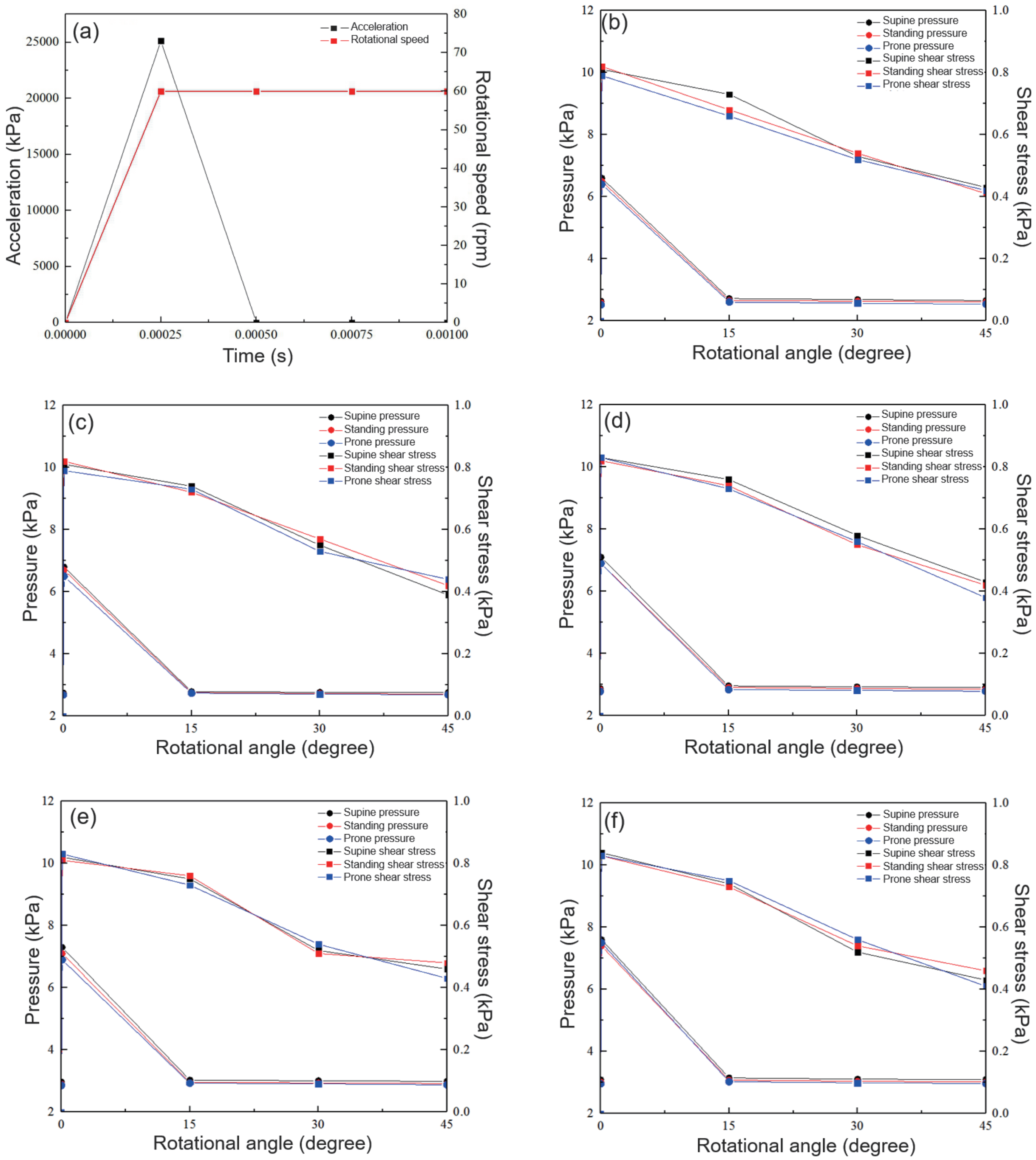

Fig. 4. (Color online) (a) Relationship between acceleration and rotational speed of eye movement and changes in IOP and shear stress with different eyeball axial lengths at a rotational speed of 150 RPM: (b) 22, (c) 24, (d) 26, (e) 28, and (f) 30 mm.

only account for the effects of corneal thickness but also include factors such as posture in the correction.

In the continuation of the simulation with fixed parameters, a probing force of 19.62 mN was used, with the corneal thickness set at 0.55 mm. Five different eye models were selected for analysis: hyperopic eyes, normal eyes with no myopia, myopic eyes with −600°, myopic eyes with −1200°, and myopic eyes with −1800°. These eye models were chosen to reflect the various effects of different refractive states on the eye's response, with the axial length adjusted according to the degree of myopia, ranging from 22 mm for hyperopia to 30 mm for −1800° myopia. Figure 4(a) shows the angular velocity and acceleration profiles of the eye. In the simulation, a constant rotational speed of 60 rpm was applied. According to the results from Fig. 4(a), the eye's acceleration reaches its maximum of 25120 rad/s^2 at 0.00025 s, after which the acceleration rapidly decreases to 0 rad/s^2, and the rotational speed stabilizes at 60 rpm. This indicates that the eye's rotational speed quickly reaches a steady state, with acceleration decreasing thereafter, consistent with the inertial properties observed in real biological systems.

Furthermore, Figs. 4(b)–4(f) illustrate the IOP and shear stress distribution for each of the five eye models (hyperopic, normal, −600° myopic, −1200° myopic, and −1800° myopic) at rotations of 15, 30, and 45°. From these figures, it is observed that the IOP increased rapidly and reached its peak when the eye rotated to approximately 0.09°. This result indicates that during eye rotation, the deformation of the cornea and internal structures causes significant changes in IOP, and as the rotation angle increases, the distributions of IOP and shear stress become more complex. The implications of these findings highlight the significant impact of the eye's structure, refractive state, and mechanical response during rotation on IOP and shear stress. Notably, the deformation of the cornea and the rotational angle of the eye are closely related. After a certain rotational angle, the internal pressure rises sharply, which could have long-term effects on eye health. This is especially relevant in myopic or highly myopic eyes, where the changes in IOP may be more pronounced. Therefore, further investigation into the dynamic changes in IOP during eye rotation is crucial for understanding ocular diseases such as glaucoma and ensuring the safety of eye surgeries.

4. Conclusions

The measurement results indicated that as the applied pressure increased to 1.33, 2.66, 3.99, 5.32, and 6.65 kPa, the strain in the cornea progressively changed to 0.091, 0.11, 0.13, 0.14, and 0.15 mm/mm, respectively, showing a gradual increase. Concurrently, the equivalent stress in the cornea also increased with the applied pressure, with values of 0.087, 0.114, 0.138, 0.177, and 0.195 MPa, respectively. The simulated IOP values for supine, standing, and prone positions, with the corneal thickness set at 0.5, 0.55, and 0.6 mm, clearly demonstrated that as the corneal thickness increased, the simulated IOP gradually decreased. In the simulation, a constant rotational speed of 60 rpm was applied. The eye's acceleration peaked at 25,120 rad/s^2 at 0.00025 s, after which it rapidly decreased to 0 rad/s^2, and the rotational speed stabilized at 60 rpm. During eye rotation, the deformation of the cornea and internal structures caused significant changes in IOP, and as the rotation angle increased, the distributions of IOP and shear stress became more complex, and the deformation of the cornea and the rotational angle of the eye were closely related.

Acknowledgments

This research was supported under Project nos. NSTC 113-2622-E-390-001 and NSTC 113-2221-E-390-011.

References

1 B. Thylefors and A. D. Negrej: Bull. World Health Organ. **72** (1994) 323.
2 What is the normal eye pressure range?: https://www.healthline.com/health/eye-health/eye-pressure-range (accessed March 2025).
3 I. A. Sigal, J. G. Flanagan, and C. Ross Ethier: Invest. Ophthalmol. Visual Sci. **46** (2005) 4189.
4 A. Shin, L. Yoo, J. Park, and J. L. Demer: ASME J. Biomech. Eng. **139** (2017) 101010.
5 J. R. Phillips and N. A. McBrien: Ophthal. Physiol. Opt. **15** (1995) 351.
6 B. Kishorea and N. P. Ananthamoorthy: Genomics **112** (2020) 3089.
7 H. Li, T. Liu, B. Mu, X. Zhao, C. Xue, M. Shen, V. Jhanji, and Y. Wang: Exp. Eye Res. **197** (2020) 108109.
8 A. F. Fuchs: J. Physiol. **191** (1967) 609.
9 S. Cai, P. C. Wu, C. C. Cheng, C. M. Hsu, L. Y. C. Poon, and C. F. Yang: Sens. Mater. **36** (2024) 4179.
10 M. Kohlhaas, A. G. Boehm, E. Spoerl, A. Pursten, H. J. Grein, and L. E. Pillunat: Arch. Ophthalmol. **124** (2006) 471.